

Arrayed narrow linewidth erbium-doped waveguide-distributed feedback lasers on an ultra-low-loss silicon-nitride platform

Michael Belt,* Taran Huffman, Michael L. Davenport, Wenzao Li, Jonathon S. Barton, and Daniel J. Blumenthal

Electrical and Computer Engineering Department, University of California, Santa Barbara, California 93106, USA

*Corresponding author: michaelbelt@ece.ucsb.edu

Received July 16, 2013; revised September 18, 2013; accepted October 16, 2013;

posted October 16, 2013 (Doc. ID 194001); published November 14, 2013

We demonstrate an array of erbium-doped waveguide-distributed feedback lasers on an ultra-low-loss Si₃N₄ platform. Sidewall gratings providing the lasing feedback are defined in the silicon-nitride layer using 248 nm stepper lithography, while the gain is provided by a reactive co-sputtered erbium-doped aluminum-oxide layer. We observe lasing output over a 12 nm wavelength range (1531–1543 nm) from the array of five separate lasers. Output powers of 8 μW and lasing linewidths of 501 kHz are obtained. Single-mode operation is confirmed, with side-mode suppression ratios over 35 dB for all designs. © 2013 Optical Society of America

OCIS codes: (140.3490) Lasers, distributed-feedback; (130.3120) Integrated optics devices; (140.3460) Lasers.

<http://dx.doi.org/10.1364/OL.38.004825>

Low-cost, high-performance integration technologies that enable a new generation of ultra-narrow-linewidth, temperature stable, and multiwavelength lasers on-chip will create a significant impact in numerous applications including coherent communications [1], high spectral resolution LIDAR systems [2], and long-range optical frequency-domain reflectometry systems [3]. A pre-eminent candidate for these new classes of lasers is the silicon-nitride ultra-low-loss waveguide (ULLW) platform [4]. Silicon-nitride-waveguide-based passive components have been shown to offer ultra-low loss, high performance, and tight fabrication tolerance for desired design parameters. Si₃N₄ strip waveguides clad by SiO₂ have demonstrated on-chip waveguide propagation loss below 0.1 dB/m [4] with coupling losses of 0.7 dB to optical fibers [4]. Just as well, the ultra-low loss of this waveguide design enables extremely long, low-coupling constant filters with the narrow passbands required for integrated low-linewidth lasers [5].

Recent efforts at integrating active elements within the ULLW platform have concentrated on bonding hybrid indium phosphide/silicon layer structures with tapered mode couplers to transfer light between the silicon and the silicon-nitride waveguides [6]. Such an approach relies on a complicated fabrication process, with tight constraints on process parameters, and precise alignment between the silicon, InP, and silicon-nitride waveguides. When compared to rare-earth-ion-doped dielectric materials, semiconductor gain media exhibit relatively wide lasing linewidths, high amplifier noise figures, and low-temperature stability. Since rare-earth-ion-doped dielectric materials do not exhibit an amplitude-phase coupling mechanism as large as that observed in semiconductor lasers, these materials can be used to realize linewidth values that would otherwise be unobtainable with standard semiconductor designs.

The erbium-doped aluminum oxide (Al₂O₃:Er³⁺) gain medium has shown the capability to act as both a broad-band, high-gain region for amplification [7], as well as a wavelength stable source for narrow-linewidth lasers [8]. From an integration perspective, the erbium-doped gain

layer can be added by way of only a single additional fabrication step on top of the few already required for the entirety of the ULLW platform. Overall, this greatly reduces the complexity of the fabrication process when compared to those necessitated by utilizing a semiconductor-based alternative. Integrating such an active medium with the functionalities created through the ULLW platform, in particular highly selective sidewall grating filters [9], allows for the realization of novel, high-performance optical communications devices.

In this Letter, we demonstrate for the first time an array of integrated Al₂O₃:Er³⁺ waveguide-distributed feedback (DFB) lasers on an ultra-low-loss Si₃N₄ platform. The devices were fabricated on 100 mm Si substrates, with sidewall grating features patterned using 248 nm stepper lithography. We observe laser output over a 12 nm wavelength range (1531–1543 nm) from the array of five separate lasers, with output powers of 8 μW and full width at half-maximum (FWHM) lasing linewidths of 501 kHz. Spectral traces show single-mode operation, with a side-mode suppression ratio (SMSR) greater than 35 dB for all designs.

The modal gain per unit length (in dB/cm) of rare-earth ion-doped media is linearly proportional to the fractional overlap (or mode confinement factor) Γ of the signal beam at wavelength λ_s within the region of the gain material being excited by the pump beam at wavelength λ_p [10]. An advantage of the extreme low loss of the nitride waveguide platform is that only a small amount of gain will be required to overcome the propagation and excess mirror losses to achieve lasing. With this in mind, we designed a waveguiding structure such that the pump and signal beams have only a small confinement factor within the Al₂O₃:Er³⁺ gain region as compared to other designs [7]. Figure 1(a) gives a schematic cross section of the material platform used in this work.

As shown, the Si₃N₄ core (thickness, $t = 79$ nm, and refractive index, $n = 1.98$) and Al₂O₃:Er³⁺ gain medium ($t = 830$ nm, $n = 1.65$) are separated by a thin layer of SiO₂ ($t = 200$ nm, $n = 1.44$). This small oxide gap provides a greater degree of freedom in tailoring the

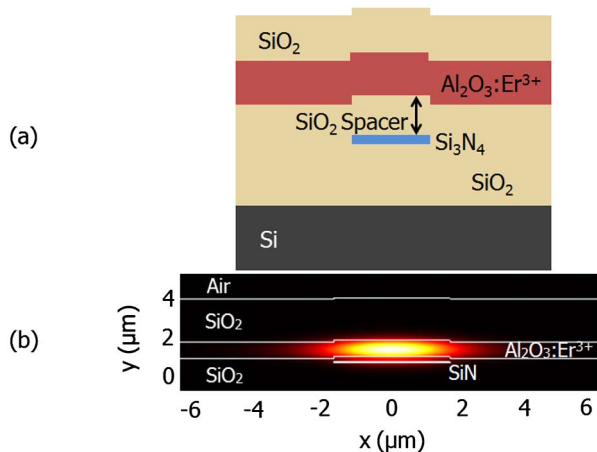


Fig. 1. (a) Cross-section diagram of the $\text{Al}_2\text{O}_3:\text{Er}^{3+}$ ULLW lasing structure. (b) Simulated TE-mode profile for the lasing light at 1531 nm.

confinement factor of the mode within the erbium-doped gain region. This cross-sectional structure is similar to the distributed Bragg reflector (DBR) design reported in [11], save for modifications of the Si_3N_4 core thickness, nominal waveguide width, SiO_2 spacer thickness, $\text{Al}_2\text{O}_3:\text{Er}^{3+}$ thickness, and presence of the top SiO_2 cladding. The net effect of the changes is a reduction in the confinement factor of the mode within $\text{Al}_2\text{O}_3:\text{Er}^{3+}$ layer. Figure 1(b) gives the simulated fundamental TE-mode profile for the 1531 nm signal, with a corresponding Γ value of 61%.

Fabrication of the devices began with 15 μm thick thermally oxidized silicon substrates measuring 100 mm in diameter. The 79 nm thick Si_3N_4 layer was deposited by low-pressure chemical vapor deposition (LPCVD) and then patterned using 248 nm stepper lithography. An inductively coupled plasma reactive-ion etch subsequently defined the nitride core. The 200 nm thick SiO_2 layer, acting as a spacer between the Si_3N_4 core and the $\text{Al}_2\text{O}_3:\text{Er}^{3+}$ active layer, was then deposited using reactive co-sputtering. The devices were then annealed in N_2 at 1050°C for 7 h. This high-temperature step was done to reduce absorption losses due to Si-H and N-H bonds around 1.52 μm [12]. The 830 nm $\text{Al}_2\text{O}_3:\text{Er}^{3+}$ gain layer was deposited by reactive co-sputtering using a process similar to that found in [13]. Finally, a 2.0 μm thick protective top PECVD SiO_2 layer was deposited. After being diced into individual die, a mechanical polishing process ensured proper conditioning of the device facets. Through optical backscattering reflectometry measurements [4], we determined the background scattering losses of undoped reference samples to be <0.25 dB/cm over the range of 1530–1600 nm. Secondary ion mass spectrometry measurements quantified the erbium dopant concentration at $1.7 \times 10^{20} \text{ cm}^{-3}$.

The DFB cavity measures 7.5 mm long, with 1 mm long \times 2.8 μm wide active input waveguides on either end between the lasing cavity and the die facet. The cavity sidewall grating is composed of periodically varying sections of alternating widths. The width difference between the two waveguide sections sets the reflection strength of the grating, or κ parameter [5]. The design set with the best performance had alternating widths of 2.56

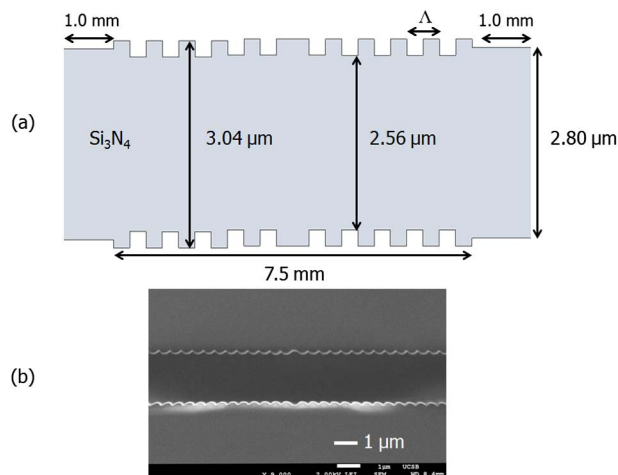


Fig. 2. (a) Top-down schematic view of the DFB laser cavity. (b) SEM micrograph of the fabricated device. The quarter-wave shift section is visible in the center of the figure. The wave-like functional form of the fabricated device differs from the intended square-like form of the device design due to an over-exposure of the photoresist during the lithography step.

and 3.04 μm , which produces a κ value of $\sim 11 \text{ cm}^{-1}$. This is shown in Fig. 2(a).

The total period length Λ , which sets the lasing wavelength of the device, is stepped between 486 and 490 nm in increments of 1 nm. This corresponds to Bragg wavelengths of 1531, 1534, 1537, 1540, and 1543 nm, respectively. Figure 2(b) shows a scanning electron microscope (SEM) image of the nitride core of a device right after the reactive ion etch fabrication step.

Figure 3 shows the experimental setup used to characterize the lasers.

Pump light from both 974 and 975 nm laser diodes is coupled onto the chip from both sides using 5 μm spot size (at the $1/e^2$ level) lensed fibers. The lasing output is collected from the 1550 nm port of a 980/1550 nm wavelength division multiplexer (WDM). The power-handling capability of the 980/1550 nm multiplexer is constrained to a maximum of 300 mW, so the output from the DFB can only be measured from the side pumped by the 200 mW 975 nm laser diode. The laser output power is measured using a power meter, while the spectrum is recorded using an optical spectrum analyzer (OSA).

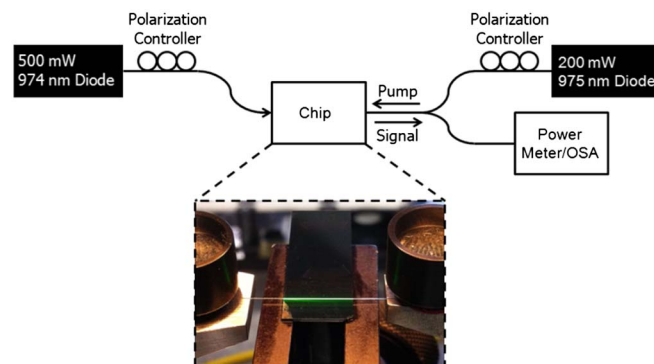


Fig. 3. Measurement setup of the experiment. The inset photo shows the device under 974 nm excitation.

In measuring the insertion loss of the devices, we estimate the coupling losses at each facet of the die to be 2.0 and 4.5 dB for the 1550 and 980 nm TE-polarized light, respectively. With this coupling loss known, we determine a maximum possible on chip pump power of 205 mW. A maximum output power of 8 μ W is obtained from the DFB laser with a center wavelength of 1543 nm. A plot of single-sided lasing output power versus pump laser input power for the device operating at 1543 nm is shown in Fig. 4.

A pump-to-signal efficiency (η) of $5.7 \times 10^{-3} \%$ is calculated for this device. The value of output power is significantly lower than the 800 μ W at 1545.2 nm obtained by the DFB in [8] when pumped with 976 nm light [14], or the 5 mW at 1561 nm obtained by the DBR in [11]. The main reason for this discrepancy is due to the differences in the total length of the devices (7.5 mm in this work compared to the 10 mm found in [8] or the 23 mm found in [11]). In rare-earth ion-doped waveguide lasers, the absorption length of the pump light poses a lower limit on how short the lasing cavity can be made, while still absorbing sufficient pump radiation to reach threshold [14]. Measurements of residual pump power captured from the end opposite the 974 nm pump diode show that the amount of pump power absorbed is ~ 1 –5%. This would mean that the low efficiency of the fabricated devices is dominantly restricted by the short cavity length. A trade-off exists here, though, as the devices cannot be made arbitrarily long. A longer cavity not only imposes a tighter constraint on the coupling constant of the grating to keep the device lasing in a single longitudinal mode, but it also experiences an upper bound set by the absorption length of the pump light. When viewed as a function of length, the loss of pump power along the cavity of an extremely long laser will eventually cause a region of the device to become highly absorbing and thus prevent laser action from occurring [15]. Optimized devices reaching 20 mm in length were fabricated, but the resolvable width differences in their sidewall gratings (and thus their realizable coupling constants) prevented them from fulfilling the required resonance condition for lasing. Further progress in this area is currently underway.

Additional improvements can be made to increase the pump-to-signal efficiency, including increasing the confinement factor of the pump light within the active region

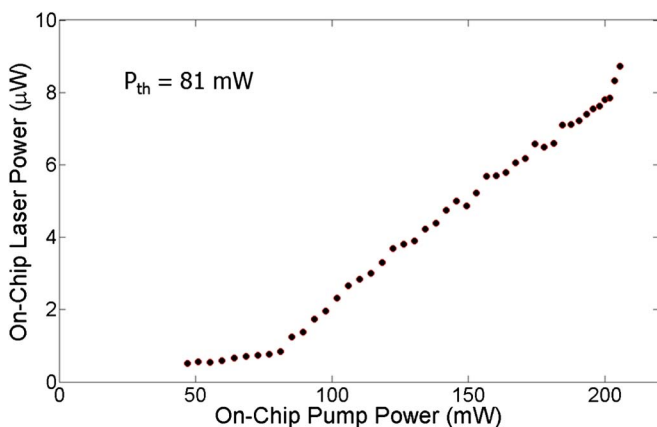


Fig. 4. On-chip single-sided lasing output power versus pump laser input power for the DFB operating at 1543 nm.

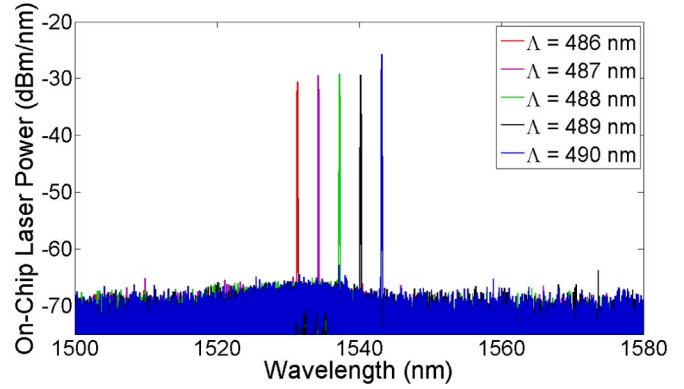


Fig. 5. Superimposed output laser spectra as measured with an OSA.

[10], accompanying an anneal to the upper protective SiO₂ deposition, lowering the overall scattering loss through additional chemical mechanical polishing (CMP) of the oxide spacer layer [11], and ytterbium sensitizing [16]. With such a low percentage of absorbed pump power, co-doping the Al₂O₃:Er³⁺ with Yb atoms could lead to more efficient pump energy conversion. On the other hand, such a technique may only make a small improvement in efficiency, as analogous fiber-based host glasses have shown a requirement of high phosphorous content to achieve efficient Yb–Er energy transfer.

Figure 5 shows the superimposed spectra of five different lasers all on a single chip as recorded by the OSA.

The differences in output power over the spectral range can be attributed in large part due to the nonuniform nature of the mechanical facet polishing as well as to differences in the small signal-gain spectrum of the erbium-doped region, although to a lesser degree. The spectral traces show single-mode operation, with an SMSR greater than 35 dB for all designs.

Characterization of the lasing linewidths of each device was carried out through standard self-heterodyne measurements, of which the experimental setup is shown in Fig. 6.

For the delay arm of the Mach–Zehnder interferometer, a length of 25 km of optical fiber was chosen to ensure that the differential delay time ($\Delta\tau$) was much greater than the coherence time of the laser (t_{coh}). Figure 7 shows the measured RF spectrum analyzer trace for the laser operating at 1537 nm.

Because it contains the noise of the frequency shifted and delayed versions of the optical lasing signal, the electrical FWHM (3 dB down from the peak) shown is twice as wide as the original laser linewidth. With this in mind, we measure the FWHM linewidth of the device as

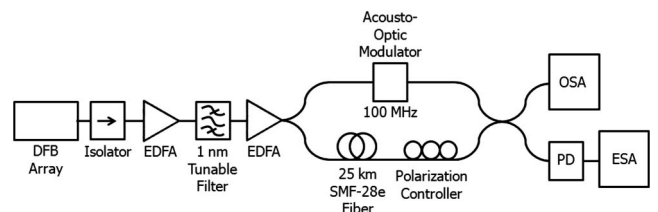


Fig. 6. Experimental setup for the self-heterodyne linewidth measurement technique.

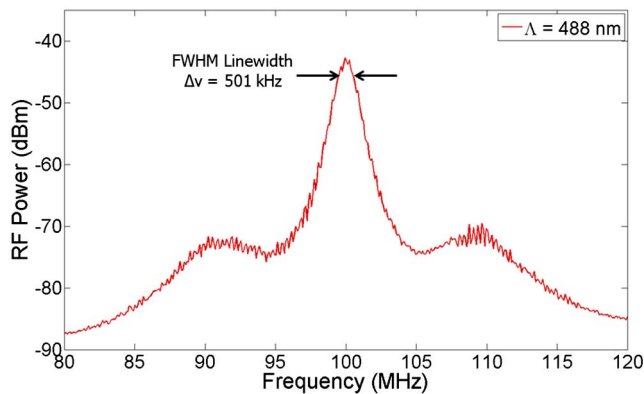


Fig. 7. Measured RF power spectrum for the laser operating at 1537 nm. For the measurement the resolution bandwidth of the ESA was set at 10 kHz.

501 kHz. The satellite peaks shown at 9 MHz on either side of the main lobe are caused by relaxation oscillations within the laser. However, the FWHM linewidth of the device is essentially the same with or without the satellite peaks present [17]. The high linewidth value of the devices (501 kHz as compared to the 1.7 kHz achieved in [8]) is mainly a consequence of the low output power of the lasers, as lasing linewidth is inversely proportional to the output power [18].

In summary, we have demonstrated an array of integrated $\text{Al}_2\text{O}_3:\text{Er}^{3+}$ waveguide-DFB lasers on an ultra-low-loss Si_3N_4 planar waveguide platform. Sidewall gratings providing the lasing feedback are defined in the silicon-nitride layer using 248 nm stepper lithography, while a simple reactive co-sputtering step deposits the erbium-doped aluminum-oxide active layer. Lasing with output powers of $8 \mu\text{W}$ at wavelengths between 1531 and 1543 nm are shown, with SMSRs greater than 35 dB and FWHM lasing linewidths of 501 kHz. Potential improvements in pump-to-signal efficiency are possible and within immediate reach, including optimizing the device length, adding an additional CMP step of the silicon-dioxide spacer slayer, ytterbium sensitizing, and increasing the confinement factor of the signal and pump light by increasing the thickness of the active region. Realization of these lasing sources on the ULLW platform allows for the exciting possibility of higher-performance-integrated optical communications devices, high spectral resolution LIDAR systems, and long-range optical-frequency domain reflectometry systems.

The authors thank M. J. R. Heck and J. E. Bowers for their guidance in designing the devices. This work was supported under the Defense Advanced Research Projects Agency (DARPA) under the EPHI (grant no. HR0011-12-C-0006) and iPhoD (grant no. HR0011-09-C-0123)

contracts. The views and conclusions contained in this document are those of the authors and should not be interpreted as representing official policies of the Defense Advanced Research Projects Agency or the U.S. government.

References

1. K. N. Nguyen, J. M. Garcia, E. Lively, H. N. Poulsen, D. M. Baney, and D. J. Blumenthal, in *Optical Fiber Communications Conference*, Technical Digest (Optical Society of America, 2012), paper OW3G.2.
2. E. W. Eloranta, *Range-Resolved Optical Remote Sensing of the Atmosphere* (Springer, 2008), Chap. 5.
3. J. Geng, C. Spiegelberg, and S. Jiang, *IEEE Photon. Technol. Lett.* **17**, 1827 (2005).
4. J. F. Bauters, M. J. R. Heck, D. D. John, J. S. Barton, C. M. Bruinink, A. Leinse, R. G. Heideman, D. J. Blumenthal, and J. E. Bowers, *Opt. Express* **19**, 24090 (2011).
5. M. Belt, J. Bovington, R. Moreira, J. F. Bauters, M. J. R. Heck, J. S. Barton, J. E. Bowers, and D. J. Blumenthal, *Opt. Express* **21**, 1181 (2013).
6. M. L. Davenport, J. F. Bauters, M. Piels, M. J. R. Heck, A. Chen, A. W. Fang, and J. E. Bowers, in *Optical Fiber Communications Conference*, Technical Digest (Optical Society of America, 2013), paper PDP5C.5.
7. J. D. B. Bradley, L. Agazzi, D. Geskus, F. Ay, K. Wörhoff, and M. Pollnau, *J. Opt. Soc. Am. B* **27**, 187 (2010).
8. E. H. Bernhardt, H. A. G. M. van Wolferen, L. Agazzi, M. R. H. Khan, C. G. H. Roeloffzen, K. Wörhoff, M. Pollnau, and R. M. de Ridder, *Opt. Lett.* **35**, 2394 (2010).
9. M. Belt, M. J. R. Heck, J. S. Barton, J. F. Bauters, J. E. Bowers, and D. J. Blumenthal, in *Optical Fiber Communications Conference*, Technical Digest (Optical Society of America, 2013), paper OTu3C.3.
10. D. Geskus, S. Aravazhi, S. M. Garcia-Blanco, and M. Pollnau, *Adv. Mater.* **24**, OP19 (2012).
11. Purnawirman, J. Sun, T. N. Adam, G. Leake, D. Coolbaugh, J. D. B. Bradley, E. S. Hosseini, and M. R. Watts, *Opt. Lett.* **38**, 1760 (2013).
12. F. Ay and A. Aydinli, *Opt. Mater.* **26**, 33 (2004).
13. K. Wörhoff, J. D. B. Bradley, F. Ay, D. Geskus, T. P. Blauwendraat, and M. Pollnau, *IEEE J. Quantum Electron.* **45**, 454 (2009).
14. E. H. Bernhardt, "Bragg-grating-based rare-earth-ion-doped channel waveguide lasers and their applications," Ph.D. dissertation (Department of Electrical Engineering, Mathematics, and Computer Science, University of Twente, 2012).
15. J. Bradley, " $\text{Al}_2\text{O}_3:\text{Er}^{3+}$ as a gain platform for integrated optics," Ph.D. dissertation (Department of Electrical Engineering, Mathematics, and Computer Science, University of Twente, 2009).
16. P. Burns, J. M. Dawes, P. Dekker, J. A. Piper, H. Zhang, and J. Wang, *IEEE Photon. Technol. Lett.* **14**, 1677 (2002).
17. L. A. Coldren, S. W. Corzine, and M. L. Mašanović, *Diode Lasers and Photonic Integrated Circuits* (Wiley, 2012), Chap. 5.
18. C. H. Henry, *IEEE J. Quantum Electron.* **QE-18**, 259 (1982).